LARGE-SCALE PECULIAR VELOCITY FIELDS IN SUPERCLUSTERS OF GALAXIES

G. GAVAZZI,[1] M. SCODEGGIO,[1] A. BOSELLI,[1] AND G. TRINCHIERI[2]

ABSTRACT

The Tully-Fisher relation is used to derive distances of 262 galaxies in seven clusters. Care is taken to reduce possible causes of error in the distance determination and to evaluate sources of scatter in the distance-velocity relation. The scatter in Virgo, A262 (and possibly in the Coma and Hercules superclusters) is real and is evidence of large-scale (50 Mpc) peculiar velocity fields. In the Virgo region we confirm the existence of background galaxies infalling toward the cluster (see work by Pierce and Tully) and we find evidence for infalling foreground objects. The Cancer cluster is confirmed to be an unbound collection of groups (see work by Bothun et al.). The Hubble relation is linear from 0 to 13,000 km s^{-1} with $H_0 = 90 \pm 17$ km s^{-1} Mpc.

Subject headings: cosmology — galaxies: clustering — galaxies: redshifts

1. INTRODUCTION

Since Tully & Fisher (1977) discovered a new method for determining distances of galaxies independent from their redshift, a significant progress was made in revealing the topology of the local universe. In particular it became possible to map the three-dimensional distribution of galaxies in the Local Supercluster (Tully & Fisher 1987). Aaronson et al. (1986, hereafter Aa86) using the infrared Tully-Fisher relation were able to derive distances of clusters of galaxies up to redshift of 11,000 km s^{-1} and confirmed the linearity of the Hubble law on this scale. The Tully-Fisher method, complemented with the Faber-Jackson relation (Faber & Jackson 1976), also revealed large-scale peculiar velocity fields in the Local Supercluster and on larger scales. The existence of condensations of matter which could act as attractors for the surrounding galaxies seems established (Dressler et al. 1987; Lynden-Bell et al. 1988), although there is not yet unanimous consent on which should be considered the "greatest" of the proposed attractors.

Since 1986 we have undertaken a multifrequency survey of nearby ($z < 0.03$) galaxies mostly in clusters (see Gavazzi 1990). We collected and obtained many H I line measurements and photometrical data in the infrared (H band) as well as in the visible bands, which we use in this paper to study the Tully-Fisher relation (TFr) in seven clusters of galaxies and in a large region in the Coma Supercluster. The aim of our work is to extend the work of Aa86 to a larger sample, and to check if the Tully-Fisher method can help us in revealing the existence of substructures or of peculiar motions in the superclusters.

2. THE METHOD

The results of this work are based on the comparison between galaxy recessional velocity and Tully-Fisher distance: TFD = dex $[-a - b \times \log (W\ \mathrm{H}\ \mathrm{I}_c) - 25 + m_c]/5$ (eq. [1]; in megaparsecs), directly derived from the TFr: $M = a + b \times \log (W\ \mathrm{H}\ \mathrm{I}_c)$. $W\ \mathrm{H}\ \mathrm{I}_c$ is the face-on 21 cm line width and m_c is the corrected magnitude in a specified photometrical system.

The data reduction procedure adopted to derive TFD are

common to the one used in Gavazzi & Trinchieri (1989). A brief outline is given in what follows.

The H I line widths used are the mean of the 20% and 50% of the peak intensity. Only best-quality data (i.e., two horn-shaped line profiles with steep edges and high signal-to-noise ratio) are used. Line widths are corrected for galaxy inclination i (see Haynes & Giovanelli 1984), derived from the axial ratio R_{25} (at the 25th mag arcsec^{-2}), taken from the literature when available, or directly estimated on the available plate material. Only objects with $i > 45°$ are used in the following analysis.

Infrared H-band magnitudes are corrected to the same values $H_{-0.5}$ (i.e., magnitude within the aperture A such that $\log (A/D) = -0.5$). The diameter D is the uncorrected major axis from the UGC catalog or measured as consistently as possible on the POSS and on CCD frames, when available. For objects with up to 4 aperture measurements we adopt the growth curves taken from Gavazzi & Trinchieri (1989) to obtain $H_{-0.5}$. If more than 4 data points are available we use a growth curve obtained by fitting the actual measurements with a second-degree polynomial. No correction for internal or galactic absorption and no K-correction has been applied to the infrared magnitudes.

V and B band total magnitudes are obtained either from aperture measurements or from CCD observations. Extrapolation to the total value is done using either the observed growth curve (if more than 4 aperture measurements are available) or the growth curves from the RC2 (de Vaucouleurs, de Vaucouleurs, & Corwin 1976). The same curves are assumed for the V and B bands. Magnitudes are corrected to the face-on values as prescribed by the RC2. We also apply corrections for internal absorption (see Haynes & Giovanelli 1984), for galactic extinction and for the K-factor as prescribed in the RC2.

3. THE SAMPLE

The optically selected sample under study is extracted from the CGCG catalog (Zwicky et al. 1963–68), and contains all galaxies with $m_p < 15.7$ (except in Virgo where $m_p \leq 14.5$) inside the contours drawn by Zwicky to define seven nearby ($z < 0.03$) clusters of galaxies: A262, A1367, A1656, A2147, A2151, Cancer, and Virgo. The sample also includes all CGCG galaxies in the Coma Supercluster regions: $11^h30 < \alpha < 13^h30$; $18° < \delta < 32°$ outside the two clusters (Coma and

[1] Osservatorio Astronomico di Brera, Via Brera 28, 20121, Milano, Italy.
[2] Osservatorio Astrofisico di Arcetri, Largo E. Fermi, 50125, Firenze, Italy.

19

TABLE 1

Number of Objects Meeting Selection Criteria, with Available H, V, and B Band Photometry

Region (1)	H (2)	V (3)	B (4)	H, V, or B (5)
Coma	124	72	70	128
A262	13	13	13	14
Cancer	19	15	15	19
Virgo	40	51	72	76
Hercules	21	21	21	25
Total	217	172	191	262

Note.—The number of objects with photometry at least in one band is also given in col. (5).

A1367). This region is dominated by relatively isolated galaxies in the bridge between Coma and A1367, and it contains background and foreground objects as well. For the present work we have restricted the sample to all disk galaxies of type later than S0a. The morphological classification was taken from the literature, when available, or determined by direct inspection to the available plate material. Furthermore we select all galaxies detected in the 21 cm H I line and with available V, B, or H magnitudes. The H I measurements were taken from the literature (references to most of them have been compiled in Huchtmeier & Richter 1989; and in Bottinelli et al. 1990) complemented by new data and several reobservations of low signal-to-noise profiles (in total 90 galaxies) obtained at Arecibo in 1991 January (Gavazzi & Scodeggio 1991). Optical and infrared magnitudes are also taken from the literature (Gavazzi, Trinchieri, & Boselli 1990; Recillas et al. 1990 a, b; Gavazzi, Kennicutt & Boselli 1991 and references therein), complemented by new measurements of aperture photometry (48 objects in the IR and 81 in the UBV) and CCD surface photometry of 20 objects, obtained for the Cancer and A262 regions (Gavazzi et al. 1991).

Altogether, the same used in this work consists of 262 galaxies, as specified in Table 1. For each region the table reports in columns (2), (3), and (4) the number of objects meeting our selection criteria and with H, V, and B band photometry available. Column (5) gives the number of objects actually used in this work, having photometry at least in one band.

Our sample contains 115 objects more than the one in Aa86. For the clusters in common we have 2–4 times more galaxies per cluster except in the Cancer region (which Aa86 have mapped well outside the Zwicky contour). The Coma Supercluster sample is unique in that it contains galaxies at large (<12 deg) distance from Coma and A1367. Our A262 data set

(not covered by Aa86) contains only 14 objects due to its declination near the limit of the Arecibo telescope.

4. CALIBRATIONS

To calibrate the TFr we use six galaxies: M33 and NGC 2366, NGC 2403, IC 2574, NGC 3031, and NGC 4236 in the M81-N2403 group. The set of calibrators does not contain M31, used by most authors, since the H band measurements of this galaxy (Aaronson, Mould, & Huchra 1980) are limited to apertures up to 1/10 of the total (optical) diameter, too small for obtaining a reliable determination of $H_{-0.5}$.

For consistency with the objects in our sample, we have recalculated and corrected the line widths and magnitudes of the calibration galaxies as discussed in § 2. Table 2 lists the values we have derived, together with the H mag. (Aaronson, Mould, & Huchra 1980) and the B_t^0 value (RC2) for reference. The different growth curves adopted (see above) and the fact that we use D instead of D_0 leads to differences of less than 0.4 mag relative to the original works.

The values of Table 2 are used to determine the slope and zero point of the TFr using five sets of distance moduli [namely, those adopted by Aa86; by Sandage & Tammann 1976; by de Vaucouleurs 1978 (the two latter increased by 0.26 mag for an adopted Hyades modulus of 3.29 mag); by Aaronson & Mould 1983 and by Pierce & Tully 1988]. The maximum difference in the obtained zero points is 0.35 mag (between the one obtained using Sandage & Tammann 1976 and the one using Aa86 distance moduli). This translates into a maximum difference in the obtained distances of 20% (see also § 6.3). The slopes obtained individually, instead, are all consistent among each other.

Table 3 gives the values of the regression parameters adopted, derived by averaging the five sets of distance moduli. Figure 1 shows the TFr for the six calibration galaxies assuming the averaged distance moduli.

Following the method of Pierce & Tully (1988), we then use Virgo galaxies to check if the slope of the TFr is consistent with that obtained from the calibration galaxies. To do so we obviously use only the small set of well-determined Virgo members (with TFD in the range 13–16 Mpc).

The apparent magnitude–line width relations found for this sample are plotted in Figure 2 together with the fit derived from the calibration galaxies, in the H, V, and B band, respectively. The slopes are remarkably consistent with those previously found. Although the scatter in the TFr might have been artificially reduced by choosing Virgo galaxies in a limited range of distances, their slope should not be altered by that choice. Furthermore, the linearity between magnitudes and

TABLE 2

Parameters for the Calibration Galaxies

Name	i	D	W H I[a] (km s^{-1})	V_t^0	B_t^0	$H_{-0.5}$	$H_{-0.5}$[b]	B_t^0[c]
NGC 2366	63°	7.6	105.0	10.29	10.71	10.83	10.84	10.67
NGC 2403	52	17.8	252.0	8.02	8.41	6.43	6.47	8.30
Ic 2574	65	12.3	102.5	10.30	10.63	10.36	10.08	10.45
NGC 3031	58	25.7	429.0	6.45	7.33	4.18	4.39	7.24
NGC 4236	69	18.6	181.5	9.06	9.34	9.32	9.33	9.09
M33	51	103.0	195.0	4.91	5.30	4.12	4.39	5.79

[a] ⟨20%–50%⟩, not corrected to face-on.
[b] From Aaronson, Mould, & Huchra 1980.
[c] From RC2.
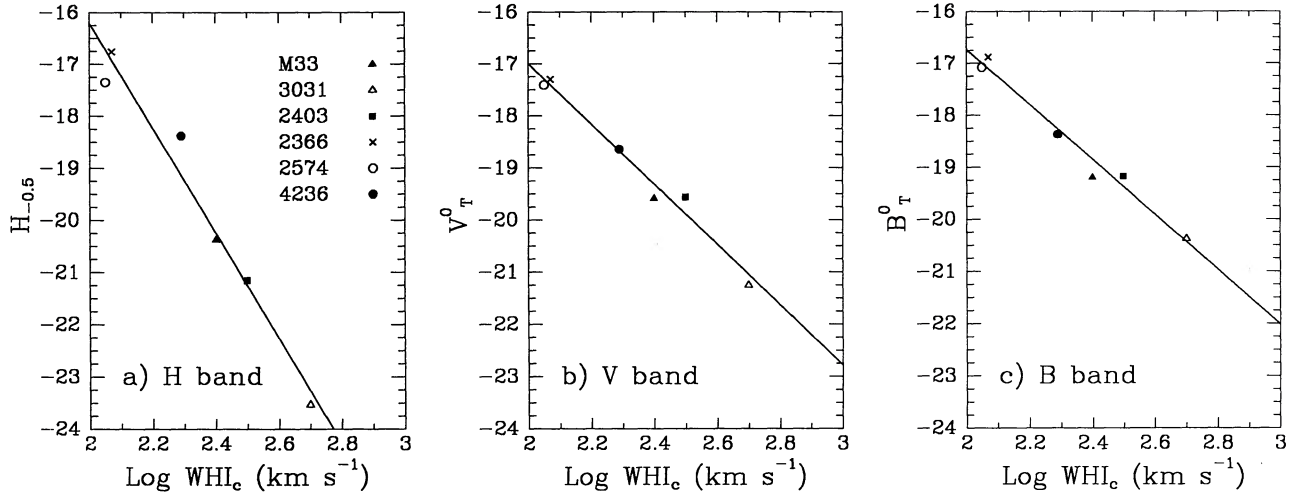
FIG. 1.—The absolute magnitude-line width relations for the calibration galaxies. The solid line represents the linear best fit to the data. (a) H band; (b) V band; and (c) B band.

line widths in both Figures 1 and 2 does not support the need for a second-order term in the solution, as adopted by Aaronson et al. (1982) and Aa86.

5. ERROR ANALYSIS

In addition to an intrinsic dispersion on the TFr (which is not well known; see, e.g., Pierce & Tully 1988), the measurement error on TFD (eq. [1]) depends upon the errors on $W H I_c$ and m_c. These are derived from the measured quantities corrected for the inclination i, which is in turn affected by the error on the measure of the axial ratio. A small dependence on the morphological type also affects the corrected B and V magnitudes.

We have assumed a typical error of 10 km s^{-1} for $W H I$, based on the improved quality of the data used here. In fact, the H I profiles are selected to be of high signal-to-noise ratio and well defined shape, and several objects have been reobserved to improve on the data quality, as explained above. To evaluate the errors on i, we have made the reasonable assumption that each axis can be measured to an accuracy of 5″ on plate material. For inclinations larger than 50°, and typical

major axes of 1′–2′, this implies an accuracy of less than 3° on i. With the above assumptions, we have estimated the errors on TFD as a function of the errors on the magnitudes, in steps of 0.1, for different i. From the error propagation analysis, we find that, in the near-infrared band, for $\sigma_m(H) < 0.4$ mag, the errors on TFD are less than 25%–30% for $i \sim 50°$, and less than 20% for $i \sim 75°$. Slightly smaller errors are expected in the V and B band, due to the shallower slope of the TFr in the optical band. Since the quoted errors on the photometric measures are ~ 0.1 mag, we evaluate a global uncertainty in the corrected total magnitudes of less than 0.4 mag to take into account uncertainties on the correction factors applied (probably smaller in the H band, where these corrections are less severe). We therefore estimate that the overall measurement uncertainty on TFD should be of $\sim 20\%$.

6. RESULTS

6.1. Comparison between V, B, and H TFD

Distances of 140 galaxies are derived simultaneously from the H, V and B data. These are not independent determinations, because they are based on the same HI line widths.
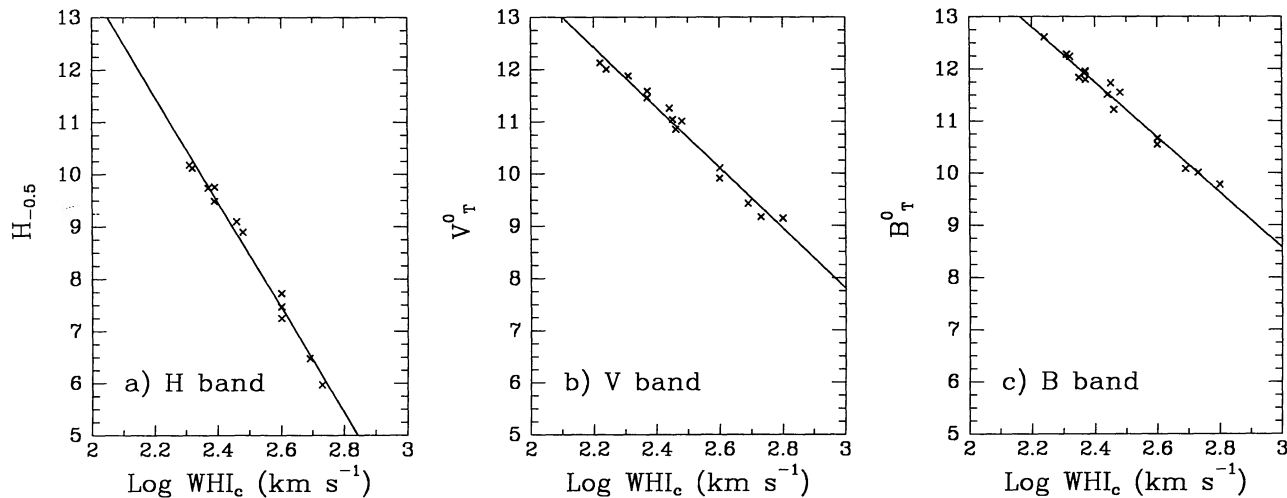
FIG. 2.—The apparent magnitude–line width relations for the subsample of Virgo members discussed in the text, used to check the slope of the TFr. The slope of the solid line is the same as in Fig. 1. (a) H band; (b) V band; (c) B band.

TABLE 3

ADOPTED LINEAR REGRESSION PARAMETERS
FOR THE TULLY-FISHER RELATION

Parameter	B	V	H
a	−6.15	−5.44	3.95
b	−5.29	−5.78	−10.08
r^2	0.97	0.98	0.97

Moreover, V and B band data might be affected by similar systematic errors since they are usually observed quasi-simultaneously.

As expected, a very tight correlation is observed between V and B band determinations. Figure 3 shows that the V and H TDF are also well correlated, with a linear regression slope of 1.1 and correlation coefficient of 0.88 (see, e.g., Pierce & Tully 1988).

Biviano et al. (1990) have shown that there are no strong reasons to prefer H band over the optical ones for determining the TFD. In light of the good correlations observed, we therefore define the TFD as the weighted mean of the H, V, and B determinations (when available). The weights assumed are 0.5 for the H band data and 0.3 each for V and B band.

6.2. Distance of Galaxies

Figure 4 shows the relation between TFD and recessional velocity for the sample galaxies, separately for each cluster or supercluster. All regions have been mapped up to 2–3 Mpc projected distance from the cluster centers. The Coma Supercluster instead has been mapped up to 20 Mpc projected distance.

The line reproduced on all plots for reference corresponds to $H_0 = 90$ km s^{-1} Mpc^{-1} (see § 6.3). The cone delimited by the dotted lines indicates the expected spread due to the uncertainty on TFD (20%). Galaxies in the cone are consistent with a pure Hubble flow within the measurement uncertainties.
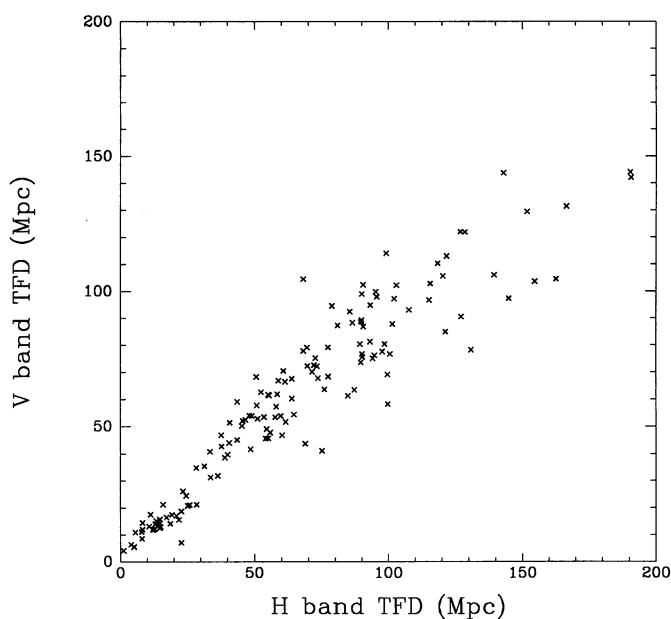
FIG. 3.—Comparison of the Tully-Fisher distances determined from the V and H bands measurements.

6.2.1. Coma Supercluster

The Coma Supercluster itself contains the Coma ($\langle V \rangle = 7153$ km s^{-1}) and A1367 ($\langle V \rangle = 6737$ km s^{-1}) clusters and the bridge of galaxies between them (Gregory & Thompson 1978). Extensive redshift surveys have been carried out in this region (Huchra et al. 1990). Figure 4a shows that in the velocity interval $6000 < V < 9000$ km s^{-1} the Hubble relation appears to have a scatter marginally larger than expected, mostly due to some galaxies lying at larger TFD relative to their velocity distance in a pure Hubble flow. These discrepant objects are all rather isolated supercluster members whereas the members of the two clusters appear to have distances compatible with their redshifts. In the foreground ($V < 6000$ km s^{-1}) and in the background ($V > 9000$ km s^{-1}) of the supercluster the data are consistent with a pure Hubble flow (see § 6.3).

The present diagram also evidences a few objects that otherwise would be included in the cluster velocity dispersion. NGC 3861 (Zw 97129), projected on A1367, suspected to be a foreground object due to its large angular size (2:4) and small redshift ($V = 5225$ km s^{-1}), and Zw 160127 ($V = 5740$ km s^{-1}), projected onto the Coma cluster, are two good examples. Similarly, the TDFs of both structures composing the legs of the "homunculus" centered on the Coma cluster (see de Lapparent, Geller, & Huchra 1986) put them in the foreground of Coma. The cloud of galaxies at the northeast of A1367 dominated by NGC 3937 has distance and recessional velocity indistinguishable from A1367 itself.

6.2.2. Hercules Supercluster

Our analysis includes the two clusters A2147 and A2151, which form the two main condensations of galaxies within the supercluster studied by Tarenghi et al. (1980) and more recently by Freudling (1990). Figure 4b shows that the broadening of the velocity-distance relation among the two cluster members is large but comparable to the expected scatter of the correlation. A similar result was obtained by Aa86.

6.2.3. A262

This elongated cluster is embedded in the ridge of galaxies in the Perseus-Pisces supercluster (Haynes & Giovanelli 1986). The cluster (Fig. 4c) shows the most significant broadening in the TFD distribution (~ 50 Mpc) in our sample. Its velocity dispersion is rather small (500 km s^{-1}), suggesting that the members of A262 have not yet reached full thermal equilibrium. This evidence indicates that A262 might be still collapsing and perhaps inducing significant peculiar motions in its surroundings. This speculation is corroborated by the spatial distribution of galaxies in the vicinity of A262, stressing the relative isolation of this cluster in space. Figures 1 and 2d in Haynes & Giovanelli (1986) in fact show that the cluster is separated from the rest of the Perseus-Pisces ridge in the east-west direction by two gaps. Furthermore their Figure 2c evidences that a significant gap occurs in the redshift distribution around 5000 km s^{-1}, precisely to the south of A262, much as if A262 swept out the galaxies from its surroundings.

6.2.4. Cancer Cluster

The Cancer cluster galaxies shown in Figure 4d are identified according to the subgrouping suggested by Bothun et al. (1983). Contrary to what is found in A262, galaxies in the Cancer region are consistent with a pure Hubble flow, as found by Aa86 and by Gavazzi, Trinchieri, & Boselli (1990). This result strongly supports the conclusion of Bothun et al. (1983),
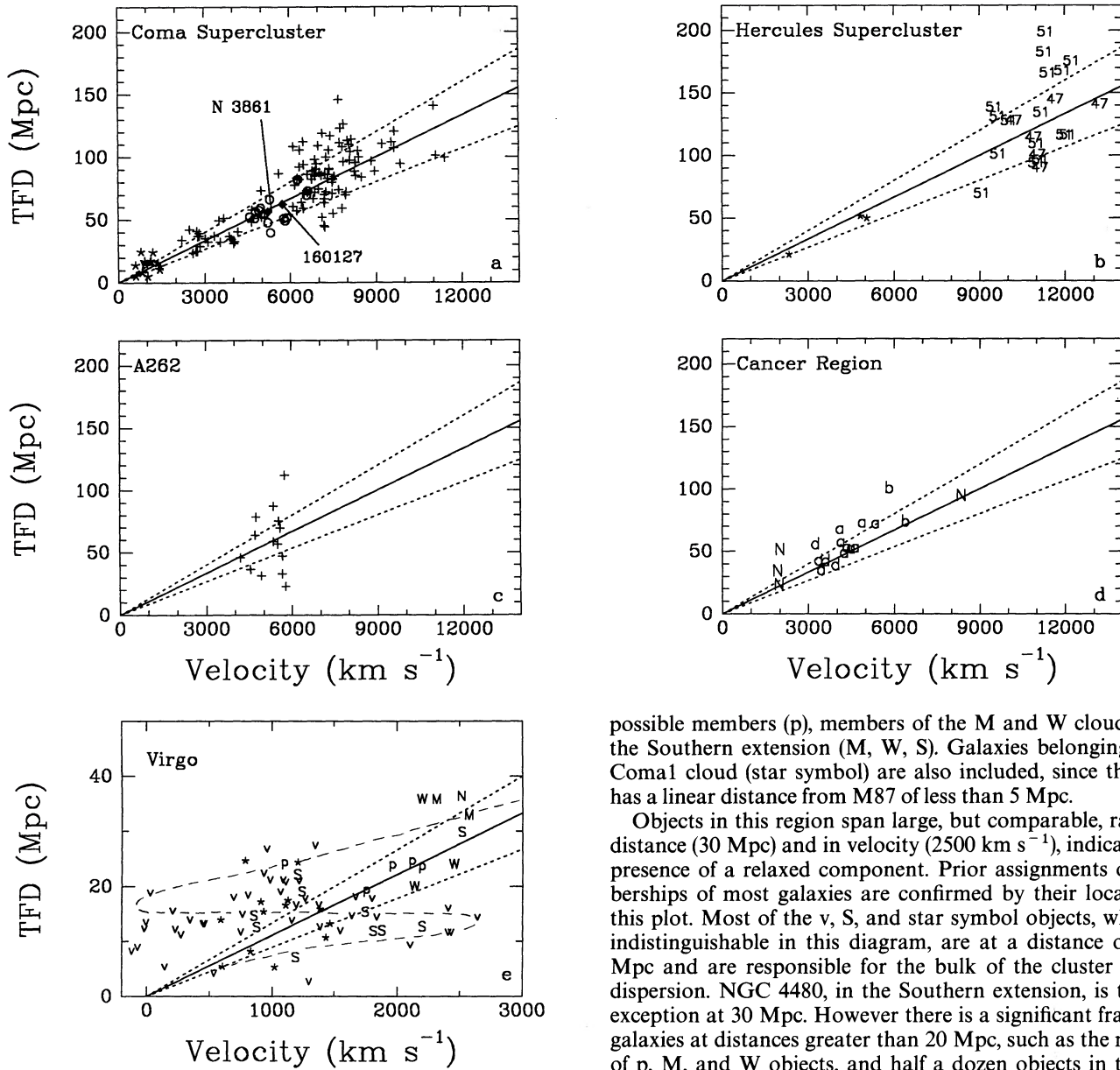
FIG. 4.—Distance-velocity relations in our sample. The line represents $H_0 = 90$ km s^{-1} Mpc^{-1} and the dotted lines the estimated uncertainty of the distance measurements (20%). (a): the Coma Supercluster region (+), Coma1 cloud (star symbol), the filaments on the foreground of the Coma cluster (open circles) and NGC 3861 and 160127. (b) The Hercules region A2147 (47), A2151 (51), and foreground objects (star symbol). (c) A262. (d) Cancer cluster group a, group b, group d, and nonmembers. (e) the Virgo cluster (V), Coma1 cloud members (★), the South cloud (S), the possible members (p), W and M cloud (W, M). The S-shaped line is adapted from Pierce & Tully (1988).

based on their analysis of the redshift distribution, that Cancer is an unbound collection of groups. Since the uncertainties in the measurements used in this paper are the same for all clusters, the fact that in the Cancer region we do not find any evidence for dispersion perpendicular to the Hubble law strengthens the positive result found in other regions.

6.2.5. Virgo Cluster

In Figure 4e, different symbols identify galaxies defined by Binggeli, Sandage, & Tammann (1985) as Virgo members (v),

possible members (p), members of the M and W cloud and of the Southern extension (M, W, S). Galaxies belonging to the Coma1 cloud (star symbol) are also included, since the cloud has a linear distance from M87 of less than 5 Mpc.

Objects in this region span large, but comparable, ranges in distance (30 Mpc) and in velocity (2500 km s^{-1}), indicating the presence of a relaxed component. Prior assignments of memberships of most galaxies are confirmed by their location on this plot. Most of the v, S, and star symbol objects, which are indistinguishable in this diagram, are at a distance of 10–20 Mpc and are responsible for the bulk of the cluster velocity dispersion. NGC 4480, in the Southern extension, is the only exception at 30 Mpc. However there is a significant fraction of galaxies at distances greater than 20 Mpc, such as the majority of p, M, and W objects, and half a dozen objects in the foreground of Virgo (distance < 10 Mpc).

The velocity-distance pattern of the Virgo cluster is consistent with the model proposed by Tully & Shaya (1984) suggesting the existence of clouds of galaxies falling onto the cluster. This model predicts that the velocity-distance diagram in Virgo follows an S-shaped envelope, illustrated in Figure 4e, which qualitatively fits the observed distribution. The pattern is also consistent with the results of Pierce & Tully (1988).

Among the foreground objects, which Pierce & Tully did not have in their sample, some (NGC 4424, NGC 4455, and NGC 4826) have their distance predictable from the Hubble law, some appear falling on the Virgo cluster (NGC 4517 and NGC 4559). Two more galaxies (NGC 4438 and NGC 4694) have TFD < 10 Mpc. However, their distance determination cannot be considered reliable with the TF method due to their peculiar H I distribution (see high-resolution H I maps in Cayatte et al. 1990).

Among the background population most galaxies, including the W and M cloud, seem to follow an unperturbed Hubble

flow. There are, however, examples of galaxies falling onto the cluster, such as NGC 4316, NGC 4451, UGC 6900, and Zw 159067.

6.3. Determination of H_0

Figure 5 shows the distribution of H_0 normalized to its average value ($\langle H_0 \rangle = 90$ km s^{-1} Mpc^{-1}) as a function of galaxy recessional velocity. The Hubble constant, $H_0 =$ velocity/TFD, is derived using the galaxy heliocentric velocity (corrected for Virgocentric infall; see Kraan-Korteweg 1986) for isolated objects. For galaxies in clusters, H_0 is derived from the mean cluster velocity. Virgo members (v), symbols, and S objects have been assumed at $\langle V \rangle = 1230$, while p, W, and M are at $\langle V \rangle = 2450$ km s^{-1}.

In Table 4 we list H_0 and its dispersion obtained in various subsamples. In the Cancer cluster and in the foreground and background of the Coma supercluster, the dispersion is comparable with the errors calculated in § 5, while it increases marginally in the Coma supercluster itself and in the Hercules region. A262 and Virgo depart significantly from the expected uncertainty, even though we have distinguished two sub-condensations in the Virgo cluster.

H_0 is constant over the whole range of velocities and the overall value is $\langle H_0 \rangle = 90$ obtained using the calibration discussed in § 4. The measurement uncertainty is 17 km s^{-1} Mpc^{-1}, obtained considering all galaxies in the Cancer region and in the foreground and background of the Coma supercluster. In addition to the instrumental uncertainty $\langle H_0 \rangle$ depends on the assumed set of distance moduli for the calibration galaxies. The maximum and minimum values of $\langle H_0 \rangle$ are 96 and 81, obtained adopting the distance moduli by Aa86 and Sandage & Tamman (1976), respectively.

Figure 5 indicates that the observed scatter in H_0 is maximum at low redshift, being dominated by those galaxies in the Virgo region discussed previously (see § 6.2) which show strong departures from the Hubble flow due to their infall toward the cluster. Some marginally discrepant galaxies at higher redshift belong to the Coma Supercluster, but a large fraction of them are in A262.

In conclusion we find that superposed to the measurement

TABLE 4

H_0 VALUES FOR EACH SUBGROUP

Subsample	$\langle H_0 \rangle$	σ
Cancer	79	16
Coma Supercluster Foreground + Background	93	17
Coma Supercluster Members	88	21
Hercules	93	24
A262	103	45
Virgo	98	57

scatter, which we estimate to be 17 km s^{-1} Mpc^{-1}, we detect large variations of H_0 due to peculiar velocities around Virgo and A262. Galaxies in the Virgo cluster should be selected with great care in order to derive unbiased values of H_0.

7. CONCLUSIONS

The results of this work are in fair agreement with those obtained by Aa86 for the five clusters in common. Moreover, our larger sample allows us to study in further details the distance distribution of individual objects within each cluster. In most aggregates studies in this work we find departures from the Hubble flow traced by background and foreground galaxies respectively decelerated and accelerated with respect to their Hubble velocity. This phenomenon extends over scales approaching 50 Mpc. The above results, if confirmed, would imply that the density ρ is larger than critical on this scale.

Peculiar motions on similar scales are not surprising. The "Great Attractor," situated at 4350 km s^{-1} from the Local Supercluster induces a streaming flow reaching a velocity up to 1000 km s^{-1} in its vicinity (Lynden-Bell et al. 1988).

Even around clusters of galaxies, peculiar motions are expected on scales of 20 Mpc radius, as predicted by the model of Kaiser (1987).

Among the clusters surveyed in our work the largest departures from the Hubble flow are observed around A262 and Virgo. However, A262 appears more stretched along the distance axis than along the velocity axis, while Virgo shows a large velocity dispersion too. This indicates that there are gal-
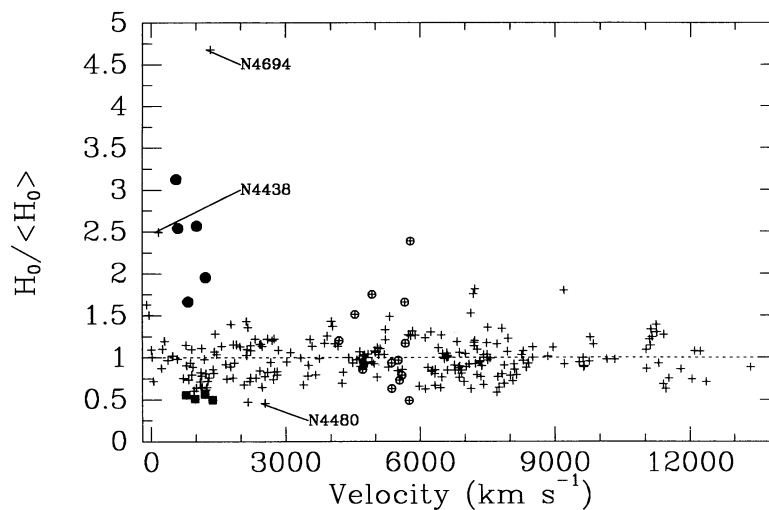
FIG. 5.—The distribution of H_0 normalized to its average value of 90 km s^{-1} Mpc^{-1}, plotted vs. recessional velocity. The broken line indicates $H_0/90 = 1$. Filled circles and filled squares represent, respectively, foreground and background galaxies falling toward Virgo. Two galaxies having unreliable TFD, as discussed in the text, and NGC 4480, in the background of Virgo, are indicated. Galaxies in A262 are marked $\oplus$.

axies gravitationally bound or falling into both clusters, but Virgo contains a much more significant virialized component. Evidence for infall toward Virgo is found also among foreground objects in addition to the ones in the background that were already discussed by Pierce & Tully (1988). Conversely, we confirm that the Cancer cluster is an unbound collection of groups, as concluded by Bothun et al. (1983) and Aa86. The null result found in Cancer and in the foreground + background of Coma, where the observed distance spread is comparable with the calculated uncertainty, strengthen the significance of the departures from the Hubble flow found in other regions.

The Hubble relation is found linear from 0 to 13,000 km s^{-1} and the value of H_0 is 90 ± 17 km s^{-1} Mpc^{-1} consistently in the H, V, and B band. This value, obtained assuming the average of five distance moduli quoted in the literature for the calibration galaxies, is consistent within the errors with those determined by Aa86 and by Pierce & Tully (1988). The quoted dispersion is purely statistical. A more fair determination of the uncertainty on H_0 from the Tully-Fisher method should also include the uncertainty on the estimate of the distance moduli used for the calibration galaxies. This, however, does not exceed 10%.

REFERENCES

Aaronson, M., Bothun, G., Mould, J., Huchra, J., Schommer, R., & Cornell, M. 1986, ApJ, 302, 536 (Aa86)
Aaronson, M., Huchra, J., Mould, J., Schechter, P., & Tully, B. 1982, ApJ, 258, 64
Aaronson, M., & Mould, J. 1983, ApJ, 265, 1
Aaronson, M., Mould, J., & Huchra, J. 1980, ApJ, 237, 655
Binggeli, B., Sandage, A., & Tammann, G. 1985, AJ, 90, 1681
Biviano, A., Giuricin, G., Mardirossian, F., & Mezzetti, M. 1990, ApJS, 74, 325
Bothun, G., Geller, M., Beers, T., & Huchra, J. 1983, ApJ, 268, 47
Bottinelli, L., Gouguenheim, L., Fouque, P., & Paturel, G. 1990, A&AS, 82, 391
Cayatte, V., Van Gorkom, J., Balkowski, C., & Kotanyi, C. 1990, AJ, 100, 604
de Lapparent V., Geller, M., & Huchra, J. 1986, ApJ, 302, L1
de Vaucouleurs, G. 1978, ApJ, 224, 710
de Vaucouleurs, G., de Vaucouleurs, A., & Corwin, H. 1976, Second Reference Catalogue of Bright Galaxies (Austin: University of Texas Press) (RC2)
Dressler, A., et al. 1987, ApJ, 313, L37
Faber, S., & Jackson, R. 1976, ApJ, 204, 668
Freudling, W. 1990, Ph.D. thesis, Cornell University
Gavazzi, G. 1990, IAU Symp. 146,
Gavazzi, G., Kennicutt, R., & Boselli, A. 1991, AJ, 101, 1207
Gavazzi, G., & Scodeggio, M. 1991, in preparation
Gavazzi, G., Scodeggio, M., Boselli, A., Garilli, B., & Trinchieri, G. 1991, A&A, submitted

Gavazzi, G., & Trinchieri, G. 1989, ApJ, 342, 718
Gavazzi, G., Trinchieri, G., & Boselli, A. 1990, A&AS, 86, 109
Gregory, S., & Thompson, L. 1978, ApJ, 222, 784
Hayes, M., & Giovanelli, R. 1984, AJ, 89, 758
———. 1986, ApJ, 306, L55
Huchra, J., Geller, M., de Lapparent, V., & Corwin, H. 1990, ApJS, 72, 433
Huchtmeier, W., & Richter, O. 1989, A General Catalogue of H I Observations of Galaxies (Berlin: Springer Verlag)
Kaiser, N. 1987, MNRAS, 227, 1
Kraan-Korteveg, R. C. 1986, A&AS, 66, 255
Lynden-Bell, D., et al. 1988, ApJ, 326, 19
Pierce, M., & Tully, B. 1988, ApJ, 330, 579
Recillas-Cruz, E., Serrano, A., Carrasco, L., & Cruz-Gonzales, I. 1990a, A&A, 229, 64
———. 1990b, preprint
Sandage, A., & Tammann, G. A. 1976, ApJ, 210, 7
Tarenghi, M., Chincarini, G., Rood, H., & Thompson, L. 1980, ApJ, 235, 724
Tully, B., & Fisher, J. 1977, A&A, 54, 661
———. 1987, Nearby Galaxy Atlas (Cambridge: Cambridge University Press)
Tully, B., & Shaya, E. 1984, ApJ, 281, 31
Zwicky, F., Herzog, E., Karpowicz, M., Kowal, C., & Wild, P. 1963–68, Catalogue of Galaxies and of Clusters of Galaxies (Pasadena: California Institute of Technology) (CGCG)